Analysis Of Photo neutron Production From The Patient During Radiotherapy Treatment Using CR 39 SSNTD

Rajesh.K.R, R.Ganapathi Raman*

Abstract: ***Most radiation treatments for curing cancer are completely non invasive. Usually patients will undergo radiation treatment to relieve symptoms and pain. The research focuses the various processes involved in generating photo neutron spectrum and dose proceeding from accelerator for treatment. The electrons are stimulated to high energies through a linear tube. These high-energy electron beams similarly treats shallow malignant growths. It tends to strike an objective to create x-ray beams for deep-seated tumor treatments. Hydrogen thyratrons are the direct current power supply for the modulator that has a pulse-forming network with switch tube. This results in a flat-topped high voltage pulse from the modulator area to DC pulse for a few microseconds of the period.Photo neutron spectrum and dose calculated. 15 MV lead to photo neutron production from many of the elements including Tungsten, Lead, Tantalum Nitrogen, Phosphorus and so on. Particularly 207Pb has photo neutron threshold as low as 6.74 MeV and 182W has threshold 8.04 MeV. Moreover, Nitrogen and Phosphorus have a lesser threshold for photo-proton emission at 7.55 MeV and 7.3 MeV respectively. Considering the radiation-weighting factor for neutrons, it is obvious that, the neutron dose considered in the treatment planning process, and we have to incorporate some mechanism in the radiotherapy treatment delivery for neutron free photons.***

Index Terms**: *Solid Cancer, linear accelerator, photo neutron, radiation, linac.***

I. INTRODUCTION

Unlike surgery and chemotherapy, most radiation treatments are completely non-invasive. Patients that cannot go through the medical surgery or chemotherapy in view of their medicinal condition typically receive radiotherapy. In radiotherapy, ionizing radiations are used to destroy the tumor cells while minimally influencing the surrounding ordinary tissue [1]. While radiation goes through the body, it will bind with the healthy tissue in addition to the tumor is a non-avoidable issue. The uncontrolled growth of tumors suggests that the majority of its cells lie in the mitotic (M) phase of the cell cycle. This turns out to be maximum radiosensitive [2].

Taking advantage of the growth properties of tumors, two different quantities of radiation therapy is established. First is Tumor Control Probability (TCP) and other is Normal Tissue Complication Probability (NTCP). The therapeutic ratio is the proportion of these two quantities for a specific radiation dose which relates the tumor response to a specific measure of surrounding ordinary tissue damage. There are two common radiation delivery techniques in radiotherapy: brachytherapy and external beam radiotherapy [3]. Brachytherapy is the administration of radiation by temporarily implanting a source into the tumor allowing greater sparing of healthy tissue and implanting permanently possible. Ultimately, the choice of treatment depends on the location, size, and type of tumor as well as patient health [4]. External beam radiotherapy is defined as radiation delivery from a source that is exterior to the body and is the most common technique that accounts for 80% of all radiation treatments. Depending on the tumor, different types of external beam radiotherapies are used for treatments. Conventional 3D conformal involves the intersection of one or more conformal-shaped beams at the tumor and IMRT (Intensity Modulated Radiation Therapy) applies many intensity-modulated beams using inverse treatment planning among the various external beam modalities [5]. For superficial tumors, orthovoltage x-ray units, with shallow depth dose curves deliver radiation with energies ranging from 10 KeV to 500 KeV. Conversely, for deep-seated tumors, linear accelerators deliver high-energy radiation ranging from 2MV to 25MV. Inevitably, while gaining the ability to reach deeper into the body, more healthy tissues are also irradiated.

Fluence explained equivalent dose and sources of photo neutrons measured in a medical accelerator [6]. The medical linear accelerator measurement of Neptun 10PC with the Mont-Carlo code emits MCNPX, the photo neutron contamination. In 1988, the American Association of

Revised Manuscript Received on July 05, 2019.

Rajesh.K.R, Department of Physics, Noorul Islam Centre for Higher Education, Kumaracoil, Kanya kumari District. Tamilnadu, India.
R.Ganapathi Raman, Department of Physics, Noorul Islam Centre for Higher Education, Kumaracoil, Kanya kumari District. Tamilnadu, India.

Physicists in Medicine (AAPM) published report 19 (TG 27) on neutron measurement around the X-ray radiotherapy high energy machines. These gave the recommendation for methods and instrumentation for neutron measurements inside and outside the linac treatment room and provide a detailed step-by-step description of these methods. Increased use of medical linac and complex treatment techniques in cancer created the need to verify the old calculation results with updated photonuclear cross section data and new Monte Carlo methods. Fast CR-39 Plastic Plate neutron dosimetry revealed the application of CR-39 in neutron dosimetry. The photo neutron dose equivalent to patients in a Siemens KD-S radiotherapy accelerator operating at 18MV was done through measurements and Monte Carlo simulations [7].

Neutron production because of photonuclear interactions in linear accelerators has been an unwanted by-product of radiotherapy treatments. Interaction of photons with materials or air produce secondary neutrons called contaminated neutrons. Compared to photons, neutrons can produce carcinogenic mutations up to twenty times more effectively and contribute additional dose to the patient during treatment. The Department of Radiation Oncology, Caritas Cancer Institute is equipped with Siemens Primus Plus linear accelerator. It has photon energies of 15MV and 6MV and electron energies of 18MeV, 15MeV, 12MeV, 9MeV and 6MeV. The maximum dose rate is 600MU/min. The Multi-leaf collimator system is fifty-eight pairs leaf MLC that gives leaf resolution of 1 cm at isocenter for 20 cm central of 40 cm x 40 cm field. In this present study neutron, CR39 solid-state nuclear track detector is used to perform the detection and Geant4 application is used to access the dose. Even though the neutron dose is less, considering its biological effects with respect to the photon dose, it has to be accounted while in the radiotherapy planning.

II. MATERIALS AND METHODS

The linac is used to accelerate charged particles from High frequency (HF) electromagnetic waves. The electrons are stimulated to high energies through a linear tube. These high-energy electron beams similarly treats shallow malignant growths. It tends to strike an objective to create x-ray beams for deep-seated tumor treatments. Hydrogen thyratrons are the direct current power supply for the modulator that has a pulse-forming network with switch tube. This results in a flat-topped high voltage pulse from the modulator area to DC pulse for a few microseconds of the period. At the same time, these pulses dispatched to a klystron or magnetron and then to the electron gun. Pulsed microwaves are created in the klystron or magnetron. It is injected towards the accelerator tube structure through a wave-guide system. The electron gun produces the proper instant electrons, which is the pulse injected into accelerator wave-guide or accelerator structure that is to be continued in a copper tube with its interior detached. In higher energy linacs, the structure of an accelerator is exceedingly long as it is positioned horizontally. The electrons were bent by means of an appropriate angle commonly around 270 or 90 degrees between the target and accelerator. The beam transport system is carried out by the way of precision bending of an electron beam. It consists of focusing coils, focusing coils and other different components.

When photons collide with a nucleus produces Photo neutrons. Figure 1 shows the setup of photo neuron production. A therapeutic photon beam composed of medical linear accelerators is used in external beam radiotherapy. An accelerating mono-energetic electron generated focuses the above-mentioned beams towards a target. The interaction of electrons with the target material causes them to decelerate and produce bremsstrahlung photons. This results in a beam of photons that can be focused on a tumor using various collimators.

At photon energies above 7MV, neutrons can be produced through interactions with materials in the linear accelerator in a process known as photo neutron production. This process can only happen when the incident photon energy is more compared to the threshold energy of (γ,n) reaction. In table 1, the thresholds are unique to each element and are calculated from the Q-value of the photonuclear reaction. Photo neutron production is a specific interaction of the more general photodisintegration. Photodisintegration is the interaction between a high energy photon and the nucleus of an absorber which can lead to the production of neutrons (γ,n), (γ,2n), protons (γ,p), alpha particles (γ,α) and a combination of (γ,np) and (γ,nα).

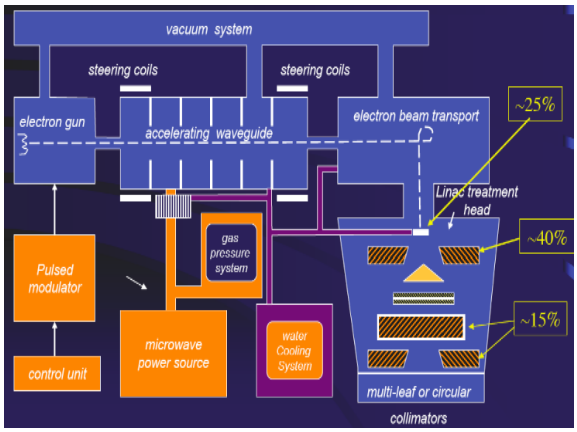

Fig.1 Setup of photo neuron production

Table 1 Threshold values of elements

Threshold [MeV]	Element

184 7.41	Tungsten
63 10.85	Copper
56 11.2	Iron
181 7.58	Tantalum
207 6.74	Lead

CR-39 is a recently discovered versatile plastic track detector. The CR-39 detectors can be located very close to a source without being damaged. Like a photographic realistic film, CR-39 is a model of an integrating detector. In the present work, we have chosen CR-39 detector that is an amorphous polymer consisting of short polyol chains joined by way of links containing diethylene glycol groups and carbonates into a dense three-dimensional network to a starting. In a track etch detector, a suitable chemical reagent preferentially attacks the damaged region to enlarge tracks. During the etching, the bulk material is attacked at a slower rate. The final geometry of the etched tracks is therefore determined in the simplest case by the simultaneous action of these two etching processes. The rate of these two etching processes is respectively designated as VT and VG. While the track etches rate VT depends on the specific ionization, both VG and VT are also dependent on the detector material, the etchant, its concentration and temperature of etching.

In figure 2, (a) Illustrates the shape of the etched track when VG ⁄ VT, (b) No track formation, as the surface was removed at a greater rate than the normal component of VT and (c) Sin VG⁄VT is the critical angle Θc above which tracks are registered. In figure 3, initially, the track grows with its known cone-like structure, characterized by the two etch velocities VT and VG. However, because of increases in track etch rate near the end of the particle track, the track walls develop small curvature. When the track etching reaches the end of the particle range, further etching just extends the track at the bulk-etching rate and the track structure turns out to be progressively lost. Therefore, for a determination of the particle range from a measurement of the etched track length, it is necessary that etching time is just sufficient to fully etch the particle trajectory, but not too much beyond that. In addition, corrections for the track enlargements due to the bulk etching have to be done.

Energetic particles and polymer structure were colloids that leave a trail of broken chemical bonds within CR-39. The tracks could be visualized by etching the film in NaOH solution with standard etching conditions of 6N, 600C, and 6Hrs with constant stirring. At the point when immersed in a concentrated alkali solution and hydroxide ions attack and break the polymer structure, etching away most of the plastic at a nominally fixed rate. In CR39 films clamped on a clipping system, which is rotated by using a rotor system and is immersed in an etching solution. Heating control is maintained by using a microcontroller. A DC generator controls rotating speed and voltage.

After the chemical etching of a detector, an optical microscope can easily scan the tracks of a particle using ordinary magnification. Using ImageJ and python programmed for ellipse fitting, the average diameter and angle of the recoil of each tracks can be calculated. A calibration graph with proton energy and track diameter is used for calculating the recoil proton energy. From the calculated average diameter using a python programmed Ellipse.2, the recoil proton energy can be calculated using the equation (0.0295956*d^2)-(1.16821*d) +12.674d, where d is the track diameter.

From the recoil proton energy, we can calculate the neutron energy by the equation 1,

$$Ep = En \cos 2\Theta \quad (1)$$

Where Ep is the energy of the recoiled proton, En is the incident neutron energy and Θ is the angle of recoil respectively. Recoil angle Θ is calculated from minor and major axes of the track ellipse. Numbers of scattering centers per unit area were calculated from the physical density and molecular composition. To get the spectral distribution of neutron, a histogram is plotted between this corrected counts and energy.The data analysis tools used are ImageJ, GNUPlot, Ellipse.2 and Exfor Data File. The microscope image of CR39 is analyzed with ImageJ software. From the image, a 2D profile of the area containing tracks was generated. Each track profiles in this area were fitted with Ellipse equation using GNUPlot. In this study, the Python compiler is used for resolving neutron energy data from chemically etched CR-39 foil microscopic image, which is used to calculate the neutron dose.

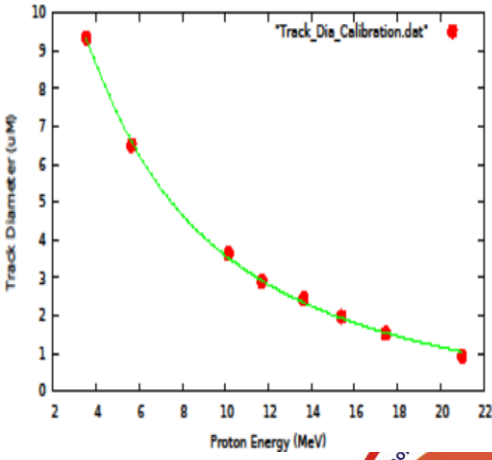

Fig.2 Calibration graph

Photonuclear reaction and therefore the cross-sections from the Geant4 database permits to simulate neutron production approximately for all nuclei and all energies from the hadron's production threshold to about 40 TeV. These characteristics, along with the capability to model complex geometries make Geant4 particularly helpful for medical linear-accelerator simulation. Carrying out the simulations also Geant4 was calculated due to the emitted photo neutrons of the patients, the most recent generation of old Geometry and Tracking. The phantom used in Geant4, of 10 × 10 × 30 cm3, made of ICRU tissue including Carbon (11 %), Oxygen (76.2 %), Hydrogen (10.1 %) and Nitrogen (2.6 %), which simulates a patient situated with its surface at 100 cm from the source. The figure 4 indicates schematically the phantom half, as used in the simulations. Dark grey cells positions were the neutron determinations are shown correspond to the axis and transver se positions are situated off an axis.

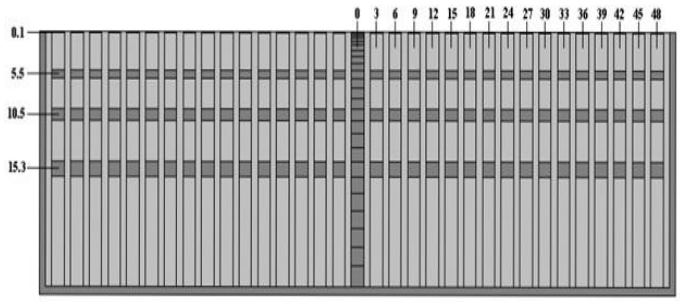

Fig.3 Dark grey cells positions in phantom half

In this work, Siemens Primus Plus linear accelerator which is in 15MV mode. The study was conducted on a patient with ca prostate treated with 3DCRT mode about a field size of 15cmx17cm. A patient is positioned on the top of the couch with an immobilization mask. A patient is aligned isocentrically. Three sets of CR39 films (1cmx1cm and density of 1.3g/cm2) one is placed on the mask at the center region of the field, one is placed on right side of the mask 5cm lateral distance from the field and one is placed 5cm inferiorly to the field. The patient planned with a box field technique with 15 MV x rays and the rate of the dose 500MU/min. The AP field is delivered with the TPS calculated MU. The same repeated for with and without the patient. The films have taken for processing. The exposed film is taken out for etching. The exposed film also etched in NaOH solution with standard etching conditions of 6N, 600C, and 6Hrs with constant stirring.

An optical microscope is used to take an image of the etched film. Formed tracks are visible under the microscope. Using Image J software we can read out the tacks and using a python programmed for ellipse fitting to count the tracks. The data also binned with a width of 250 KeV and intrinsic corrections applied by accounting elastic scattering cross section (σ). Cross section data are collected from EXFOR-ENDF (Evaluated Nuclear Data File). The midpoint of each bin is taken as the average energy (E). A number of scattering centers per unit area calculated from the physical density and molecular composition. Counts in each bin were divided with the value of (n σ) to get the real number of neutrons per energy bin, (ϕ(E))To get the spectral distribution of neutron, a histogram is plotted between this corrected counts and energy. A Geant4 application measures the neutron dose to the patient by the ICRU simulation phantom. Cross-section corrected counts and average energy are the input of the Geant4 simulator.Geant4 simulator calculates the dose due to each neutron with a given energy.

III. RESULTS AND DISCUSSION

Photo neutron spectrum and dose calculated. 15 MV lead to photo neutron production from many of the elements including Tungsten, Lead, Tantalum Nitrogen, Phosphorus and so on. Particularly 207Pb has photo neutron threshold as low as 6.74 MeV and 182W has threshold 8.04 MeV. Moreover, Nitrogen and Phosphorus have a lesser threshold for photo-proton emission at 7.55 MeV and 7.3 MeV respectively. Thus, the patient will be exposed to heterogeneous neutron energies from linac. This will add the contributions from patient supporting accessories. Further fast neutron may induce secondary neutron emission within the body. Neutrons produced in the tumor also will interact with peripheral tissues.

The energy of the recoiled protons has been estimated using track diameter - energy calibration for protons in standard etching conditions (6N NaOH, 600C, 6Hrs) and the energy of incident neutrons was deducted as above. This process was repeated to each track containing the area. A profile of overlapping tracks analysed separately as follows. The track profile was first fitted with multiple Gaussian using a software program 'Candle' and the FWTM for each individual tracks were determined. Multiple ellipses were fitted with the equation for an individual constituent track by keeping previously evaluated FWTM as a reference and are analysed. In order to confirm that no characteristic's neutrons are missed from the observation in one field of view, Images for three fields of views are recorded in this way and summed over the views and the average is calculated for one field of view. However, in this percent observation, there is no characteristic missing is observed. The difference observed is well within the statistical fluctuation of less than 4%.

The data also binned with a width of 250 KeV and intrinsic corrections applied by accounting elastic scattering cross-section (σ). Cross-section data collected from EXFOR-ENDF

(Evaluated Nuclear Data File). The midpoint of each bin is taken as the average energy (E). A number of scattering centers per unit area have calculated from the physical density and molecular composition. Counts in each bin were divided with the value of (n σ) to get the real number of neutrons per energy bin, (ϕ(E))To get the spectral distribution of neutron, a histogram is plotted between the corrected counts and energy as shown in figure 5.

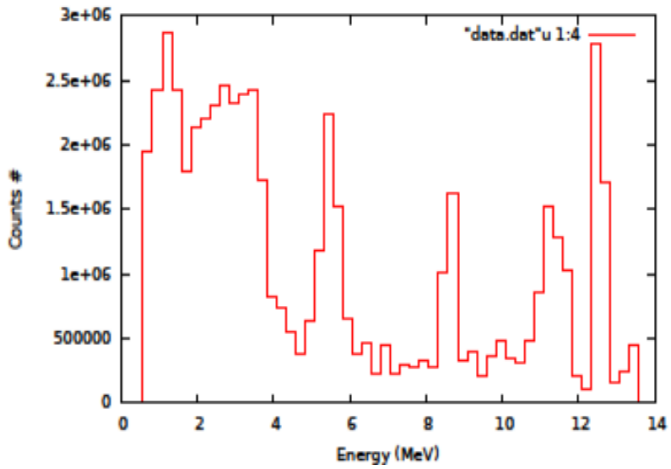

Fig.4 Histogram between the corrected counts and energy

The spectrum shows there are some of the significant amounts of high energy neutrons produced from the treatment head. The tracks due to scattered and secondary neutrons as well as low energy (<0.7 MeV) are lost on etching. This leads to loss of information about the low energy neutrons produced. An alternative mechanism is to be employed for recording low energy primary neutrons. This is important as the typical radiation-weighting factor in this energy range is 20. However, contaminations due to secondary's and scattered neutrons could be very well eliminated thereby providing data on direct neutrons. Recoil energy of the residual nucleus is found to be less than 1 KeV it will not affect the resolution of the characteristics of the neutron spectrum and hence can be neglected.

From the observed neutron peaks in the above spectra, the reaction channels were identified taking into account the various reactions having resonance reactions in the photon energy domain for elements of interest that are expected to be present in various components of treatment head. From the calculated neutron energy and counts, using Geant4 application, the neutron dose to the patient is measured.

IV. CONCLUSION

The photo neutron spectrum and dose proceeding from a medical linear accelerator are calculated. 15 MV Medical Linear Accelerator shows a significant amount of neutrons produced from (ϒ,n) reactions occurs at various parts of the machine. The consequence demonstrates which neutron dose equal from photo neutrons to patients in a conventional of the linac treatment ought not to be ignored even though it is less compared with the photon dose. The neutron dose equivalent, at the isocenter, also represents a risk for the healthy tissues and contributes to secondary malignancy insurgence. Neutron field assessment is in this way important to improve the treatment. The present technique, consisting of Geant4 simulation, can represent a reliable tool. The information likewise is used to assess the surrounding portion equal from photo neutrons to a patient accepting radiation treatment by a linear accelerator. Considering the radiation-weighting factor for neutrons, it is obvious that, the neutron dose considered in the treatment planning process, and we have to incorporate some mechanism in the radiotherapy treatment delivery for neutron free photons.

REFERENCES

1. Allen PD, Chaudhri MA. Photoneutron production in tissue during high energy bremsstrahlung radiotherapy. Physics in Medicine & Biology. 1988 Sep;33(9):1017.

2. Cyriac TS, Musthafa MM, Raman RG, Haneefa KA, Bhasi S. Out-of-field photon dosimetry study between 3-D conformal and intensity modulated radiation therapy in the management of prostate cancer. International Journal of Radiation Research. 2015 Apr 1;13(2):127-34.

3. Kry SF, Salehpour M, Followill DS, Stovall M, Kuban DA, White RA, Rosen II. Out-of-field photon and neutron dose equivalents from step-and-shoot intensity-modulated radiation therapy. International Journal of Radiation Oncology* Biology* Physics. 2005 Jul 15;62(4):1204-16.

4. Kry SF, Salehpour M, Titt U, White RA, Stovall M, Followill D. Monte Carlo study shows no significant difference in second cancer risk between 6-and 18-MV intensity-modulated radiation therapy. Radiotherapy and Oncology. 2009 Apr 1;91(1):132-7.

5. Rivard MJ, Coursey BM, DeWerd LA, Hanson WF, Saiful Huq M, Ibbott GS, Mitch MG, Nath R, Williamson JF. Update of AAPM Task Group No. 43 Report: A revised AAPM protocol for brachytherapy dose

calculations. Medical physics. 2004 Mar;31(3):633-74

6. Niroomand-Rad A, Blackwell CR, Coursey BM, Gall KP, Galvin JM, McLaughlin WL, Meigooni AS, Nath R, Rodgers JE, Soares CG. Radiochromic film dosimetry: recommendations of AAPM radiation therapy committee task group 55. Medical physics. 1998 Nov;25(11):2093-115.

7. Barquero R, Edwards TM, Iñiguez MP, Vega-Carrillo HR. Monte Carlo simulation estimates of neutron doses to critical organs of a patient undergoing x-ray LINAC-based radiotherapy. Medical physics. 2005 Dec;32(12):3579-88.

AUTHORS PROFILE

Rajesh K.R, Research scholar, Department of Physics, Noorul Islam Centre for Higher Education, Kumaracoil, Kanya kumari District. Tamilnadu, India.

R. Ganapathi Raman, Associate Professor, Department of Physics, Noorul Islam Centre for Higher Education, Kumaracoil, Kanya kumari District, Tamilnadu, India.